Hydrogen-induced oxide-to-metal charge transfer modifies catalytic sites

Downloaded from: https://research.chalmers.se, 2026-11-07 11:00 UTC

Citation for the original published paper (version of record):
Svensson, R., Grönbeck, H. (2026). Hydrogen-induced oxide-to-metal charge transfer modifies catalytic sites. Catalysis Science and Technology, 16(16): 5279-5288.
http://dx.doi.org/10.1039/d6cy00643d

N.B. When citing this work, cite the original published paper.

research.chalmers.se offers the possibility of retrieving research publications produced at Chalmers University of Technology. It covers all kind of research output: articles, dissertations, conference papers, reports etc. since 2004. research.chalmers.se is administrated and maintained by Chalmers Library

(article starts on next page)

Catalysis Science & Technology

ROYAL SOCIETY OF CHEMISTRY

PAPER

Published on 10 July 2026
Licensed under CC-BY 4.0

Check for updates

Cite this: *Catal. Sci. Technol.*, 2026, **16**, 5279

Hydrogen-induced oxide-to-metal charge transfer modifies catalytic sites

Rasmus Svensson* and Henrik Grönbeck*

Received 12th May 2026,
Accepted 8th July 2026

DOI: 10.1039/d6cy00643d

rsc.li/catalysis

Prototypical catalysts are realized as metal nanoparticles supported on a metal–oxide. It is well-known that the choice of support may have significant consequences on the catalytic activity, also in cases where the reaction is believed to occur on the metal phase. The underlying reason for this metal/oxide synergy is poorly understood, and often attributed to processes occurring at the metal/oxide interface. Here, we use density functional theory calculations to investigate the synergy between metal nanoparticles (Cu, Pd, Pt, and Au) and oxide supports (ZnO, MgO and ZrO_2) in the case of hydrogen (H_2) adsorption. The presence of a metal phase favors the formation of OH-groups in the oxide surface owing to a significant oxide-to-metal charge transfer, effectively charging the metal nanoparticles. The phenomenon is general and the hydrogen adsorption energy depends on the choice of oxide. For Cu, Pd, and Pt supported on ZnO, we find that the presence of a metal nanoparticle is crucial for the kinetics of H_2 adsorption. H_2 dissociates on the metal and occupies the oxide sites *via* a spillover mechanism. The hydrogen-induced charging of metal particles and formation of OH-groups advance the understanding of composite metal/oxide systems, with implications for catalytic properties.

Introduction

Heterogeneous catalysts are often constituted as transition metal nanoparticles (NPs) supported on porous oxides.[1] It is well-known that the support can influence the activity and selectivity in catalytic reactions.[2–4] Examples where the support affects the catalytic performance include CO oxidation,[5,6] oxygen reduction to H_2O_2,[7,8] alcohol oxidation to aldehydes,[7] hydrogenation of CO_2 to methanol,[9] and the water-gas shift reaction.[10–12] Effects of the oxide support on the catalytic performance is commonly assigned to processes occurring at the interface between the metal NPs and the support.[13,14] However, the metal/oxide synergy may extend further than the interface atoms. The support can, for example, induce strain in the supported metal NPs,[15,16] and thereby change the adsorption energies and catalytic properties.[17–19] The metal/oxide synergy could also originate from a separation of the reaction, where some elementary reaction steps occur on the support, whereas other processes occur on the metal NPs. One example is hydrogen adsorption, where hydrogen, after dissociating on the metal particle, diffuse (spillover) to the oxide surface.

On pristine oxides, H_2 may adsorb in two different configurations.[20] Heterolytic adsorption ($H_2 \rightarrow H^+ + H^-$) results in the formation of one OH-group, and one hydride-ion bound to the cation. Homolytic adsorption ($H_2 \rightarrow 2H^+ + 2e^-$) instead results in two OH-groups and two excess electrons. For irreducible oxides (the term is here used for oxides where the cations only have one oxidation state), the excess electrons are delocalized in the conduction band of the oxide,[21] whereas for reducible oxides the excess electrons give rise to changes in the cation oxidation states. Heterolytic adsorption is favored on bare ZnO,[22,23] MgO,[24] and ZrO_2,[25] whereas homolytic adsorption is preferred on reducible oxides, such as CeO_2.[26]

It is possible that the mere presence of a metal phase affects stability of hydrogen adsorption on oxides. Previous calculations of thin oxide films supported on metals[27,28] have shown that homolytic adsorption of hydrogen can be stabilized on irreducible oxides *via* charge transfer across the oxide film. The metal is for these inverse catalysts acting as an electron reservoir. It is, however, not clear how hydrogen adsorbs in conventional catalyst configurations with metal NPs supported on an oxide.

Here, density functional theory (DFT) calculations are used to investigate H_2 adsorption on mixed metal/oxide systems composed of Cu, Pd, Pt, and Au NPs supported on irreducible ZnO($10\bar{1}0$), MgO(100), and (tetragonal) tr-ZrO_2(101) surfaces. On the bare oxides (in the absence of a metal NP), hydrogen is adsorbed weakly in a heterolytic fashion. The presence of a supported metal NP changes the situation by a significant oxide-to-metal charge transfer. The adsorption is stabilized and homolytic adsorption is the preferred configuration. In addition

Department of Physics and Competence Centre for Catalysis, Chalmers University of Technology, SE-412 96 Göteborg, Sweden. E-mail: rassve@chalmers.se, ghj@chalmers.se

to stabilizing dissociative H_2 adsorption, the metal NP also affects the kinetics, as a spillover mechanism of H from the metal NP to the oxide support is favored over direct H_2 dissociation on the oxide. The metal-facilitated adsorption of H_2 on the oxide support results in new interface sites, with OH-groups close to negatively charged metal NPs. The results are general and could have important consequences for the catalytic activity of the systems.

Methods

Density functional theory calculations are performed using the Vienna *Ab Initio* Simulation Package (VASP).[29–32] The interactions between the core- and valence electrons are described by the frozen core projector augmented wave (PAW) method.[33,34] The considered valence electrons are $1s^1$ (H), $2s^2 2p^4$ (O), $3s^2$ (Mg), $3d^{10}4s^1$ (Cu), $3d^{10}4s^2$ (Zn), $4s^2 4p^6 4d^3 5s^1$ (Zr), $5s^1 4d^9$ (Pd), $6s^1 5d^9$ (Pt), and $6s^1 5d^{10}$ (Au). The functional by Perdew, Burke and Ernzerhof (PBE) is employed to describe the exchange and correlation effects.[35] In the case of ZnO and ZrO_2, Hubbard-U values of 7.5 eV and 4.0 eV are assigned to the Zn-3d and Zr-4d electrons, respectively,[36–38] to reduce electron over-delocalization. The plane waves are truncated at 500 eV in the expansion of the Kohn–Sham orbitals. The electronic structure is considered converged when the changes in electronic energy and Kohn–Sham eigenvalues are below 1×10^{-6} eV between succeeding iterations. The optimization of geometries are performed using the conjugate gradient method, until the maximum force is below 0.03 eV Å^{-1}.

The oxide supports are modeled using surfaces of $p(6 \times 5)$ wurtzite ZnO(10$\bar{1}$0), $p(6\sqrt{2} \times 6\sqrt{2})$R45° MgO(100), and $p(4 \times 6)$ tetragonal (tr-)ZrO_2(101). For ZnO, the slab is constituted of four atomic layers, of which the bottom two layers are kept fixed to emulate a bulk system. For MgO and ZrO_2, the slabs are constituted of three layers, with the bottom layer fixed to the corresponding bulk positions. The periodic slabs are separated by at least 22 Å of vacuum. Atomic models of the considered metal oxides with a supported 54-atom Pt truncated octahedron NP are presented in Fig. 1. The Brillouin zone is sampled by the Γ-point. Gas phase H_2 is calculated in a (30, 31, 32) Å vacuum box. The vibrational modes of adsorbed and gaseous hydrogen is obtained assuming the harmonic approximation, and calculated using finite differences. The average zero-point corrected (ZPC) adsorption energy of nH_2 is calculated as

$$\bar{E}_{\mathrm{ads}}(n\mathrm{H_2}) = \frac{1}{n}\left(E^{\mathrm{ZPC}}(\mathrm{system} + 2n\mathrm{H}) - E^{\mathrm{ZPC}}(\mathrm{system}) - nE^{\mathrm{ZPC}}(\mathrm{H_2(g)})\right). \quad (1)$$

Bader charge analyses are used to investigate the charge distribution in the considered systems.[39] Transitions state configurations are obtained using the climbing image nudged elastic band (CI-NEB) method,[40,41] and transitions states are verified by vibrational mode calculations. For the nudged elastic band calculations of the Pt/ZnO system, the surface is modeled using a $p(6 \times 4)$ ZnO(10$\bar{1}$0) surface constituted of three atomic layers, of which the bottom layer is kept fixed to the corresponding bulk positions. For the CI-NEB calculations on Cu/ZnO and Pd/ZnO, the $p(6 \times 5)$ cells, constituted of four atomic layers are used.

Results

The adsorption of hydrogen on the oxide supports is explored by investigating the adsorption of H_2 on bare ZnO(10$\bar{1}$0), MgO(100), and tr-ZrO_2(101). The influence of a metal is investigated by H_2 adsorption on ZnO(10$\bar{1}$0) in the presence of Cu, Pd, Pt, and Au NPs, both at low and high hydrogen coverages. A 54-atom Pt NP is used to investigate the metal/metal–oxide synergy upon H_2 adsorption for different oxides, namely ZnO(10$\bar{1}$0), MgO(100), and tr-ZrO_2(101). Lastly, the barrier for H_2 dissociation and spillover from the metal to the oxide is studied for Cu, Pd, and Pt supported on ZnO(10$\bar{1}$0).

Adsorption of H_2 on bare metal–oxides

The adsorption of H_2 is investigated on bare ZnO(10$\bar{1}$0), MgO(100), and tr-ZrO_2(101). Heterolytic adsorption results in the formation of one OH-group and one cation-H bond. Homolytic adsorption results instead in the formation of two

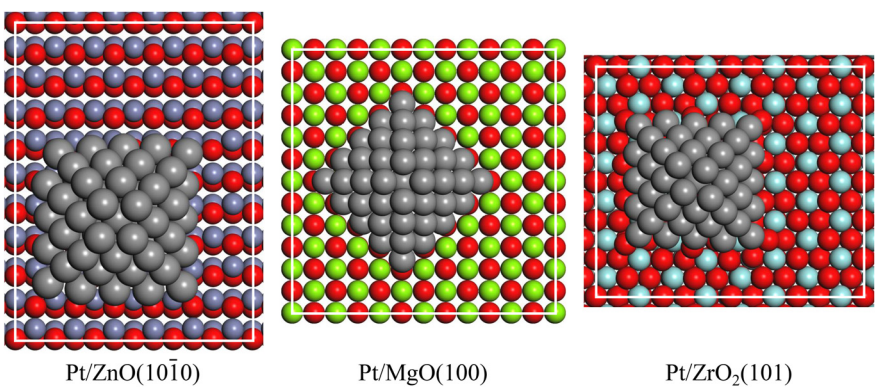

Fig. 1 Atomic models of the optimized structures of the 54-atom Pt NP supported on ZnO(10$\bar{1}$0) [left], MgO(100) [middle], and tr-ZrO_2(101) [right]. Atomic color codes: red (O), green (Mg), blue (Zn), light blue (Zr), and gray (Pt).

 This journal is © The Royal Society of Chemistry 2026

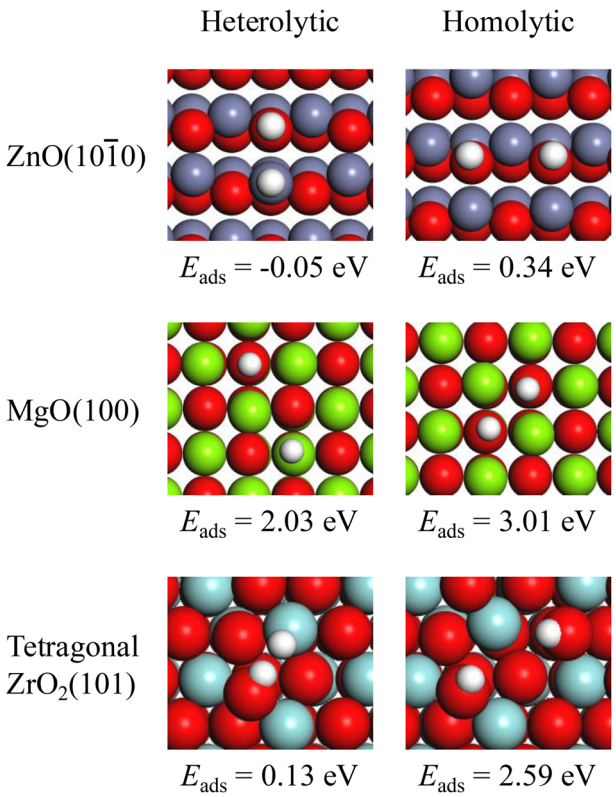

Fig. 2 Heterolytic (left) and homolytic (right) adsorption of H_2 on ZnO(10$\bar{1}$0) (top), MgO(100) (middle), and tr-ZrO_2(101) (bottom). The corresponding adsorption energy is presented below each structure. Note that the heterolytic adsorption is favored in all cases. Atomic color codes: white (H), red (O), green (Mg), blue (Zn), and light blue (Zr).

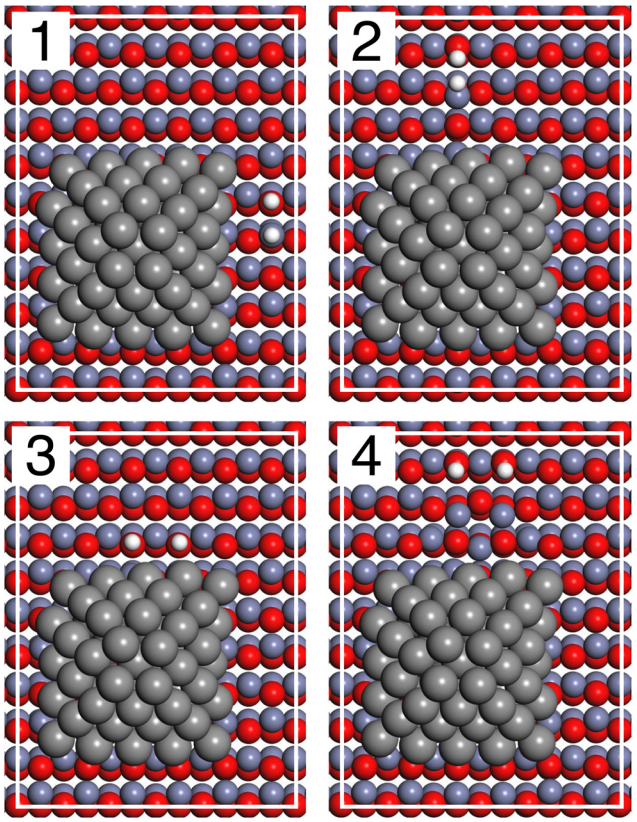

Fig. 3 Optimized adsorption configurations on Pt/ZnO(10$\bar{1}$0). The adsorption configurations are: (1) heterolytic adsorption close to the metal NP, (2) heterolytic adsorption far from the metal NP, (3) homolytic adsorption close to the NP, and (4) homolytic adsorption far from the NP. Atomic color codes: white (H), red (O), blue (Zn), and gray (Pt).

OH-groups (and two excess electrons). The optimized adsorption configurations on the three oxides are presented in Fig. 2. The heterolytic adsorption is favored over the homolytic adsorption in all cases. On ZnO, the heterolytic adsorption energy with respect to H_2 in the gas-phase is −0.05 eV (exothermic), whereas the homolytic adsorption energy is 0.34 eV (endothermic). The homolytic adsorption configuration in Fig. 2 has the two OH-groups along a ZnO row and the H–H distance is 3.38 Å. Another homolytic configuration where H occupies sites 5.19 Å apart across the ZnO rows (see Fig. S18) has an adsorption energy of −0.02 eV. The adsorption of hydrogen is significantly weaker on MgO, with a heterolytic adsorption energy of 2.03 eV and a homolytic adsorption energy of 3.01 eV. The preference for heterolytic adsorption is further emphasized on ZrO_2, where the heterolytic adsorption energy is 0.13 eV, whereas the homolytic adsorption energy is 2.59 eV. The preference of heterolytic adsorption on the three oxides is in agreement with infra-red spectroscopy measurements[22–25] and previous calculations.[21,28]

Adsorption of H_2 on M/ZnO

To investigate the influence of a supported metal NP on the adsorption properties of H_2, NPs constituted of 54 atoms of Cu, Pd, Pt, and Au are added to the ZnO(10$\bar{1}$0) surface. Four different adsorption configurations of H_2 are investigated. The investigated configurations are: (1) heterolytic adsorption close to the metal NP, (2) heterolytic adsorption far from the metal NP, (3) homolytic adsorption close to the metal NP, and (4) homolytic adsorption far from the metal NP. The different adsorption configurations are presented in Fig. 3 in the case of Pt/ZnO(10$\bar{1}$0). The adsorption energies of H_2, and the corresponding transferred charge to the metal NP for the different adsorption configurations are presented in Table 1.

The heterolytic adsorption of H_2 close to the metal NP is only slightly affected (~0.1 eV) as compared to the heterolytic adsorption on the bare ZnO(10$\bar{1}$0) surface. Heterolytic adsorption further away from the NP is slightly more exothermic, as a result of oxide distortions. Neither of the heterolytic adsorption configurations result in any significant charge transfer for any of the different NPs, regardless of the metal. The situation is significantly changed in the case of homolytic adsorption (forming two OH-groups and two excess electrons). Homolytic adsorption close to the metal NPs is exothermic (−1.45–−1.91 eV) for the four metals. In the presence of a supported metal NP, the excess electrons, stemming from the homolytic adsorption, are transferred to the metal. The homolytic adsorption further away from the

Table 1 The adsorption energy and charge transferred to (positive value) and from (negative value) the supported metal NP for the different adsorption configurations: (1) heterolytic adsorption close to the NP, (2) heterolytic adsorption far from the NP, (3) homolytic adsorption close to the NP, and (4) homolytic adsorption far from the NP. A positive value represents electrons transferred to the NP

	Heterolytic		Homolytic	
System	1	2	3	4
Cu/ZnO($10\bar{1}0$)	0.06 eV/−0.02 e	0.00 eV/−0.02 e	−1.84 eV/0.17 e	0.10 eV/0.40 e
Pd/ZnO($10\bar{1}0$)	0.06 eV/0.27 e	−0.08 eV/0.29 e	−1.45 eV/0.93 e	0.15 eV/0.77 e
Pt/ZnO($10\bar{1}0$)	0.06 eV/−0.04 e	−0.22 eV/−0.02 e	−1.91 eV/0.76 e	−0.61 eV/0.56 e
Au/ZnO($10\bar{1}0$)	0.01 eV/0.10 e	−0.09 eV/0.10 e	−1.78 eV/0.85 e	−0.53 eV/0.85 e
ZnO($10\bar{1}0$)	−0.05 eV		0.34 eV	

metal NPs are also more energetically favorable as compared to the homolytic adsorption on the bare ZnO($10\bar{1}0$) surface. However, the effects are not as pronounced as the adsorption close to the metal NPs. The main reason for the smaller effects further away from the NP is the weaker Coulomb interactions between H^+ and the negatively charged metal NP. In the case of Pt and Au particles, the homolytic adsorption results in a slight distortion of the ZnO($10\bar{1}0$) surface, resulting in a stronger adsorption energy. The charge transfer upon the homolytic adsorption of H_2 is lowest for Cu, which is related to the comparably low work function of Cu. Note that the adsorption energy of H_2 does not only depend on the metal work function, as slight distortions of the oxide surface also affects the adsorption energies. However, the significantly more favorable homolytic adsorption in the presence of a NP is general for all investigated metals. Hence, the oxide sites close to the metal NPs are expected to be covered with H, resulting in an altered interface as compared to both the metal particles and the bare metal oxide.

The oxide-to-metal charge transfer upon the adsorption of H_2 is similar to the charge transfer occurring across thin metal supported oxide films[27,42–45] and upon the adsorption of hydrogen at the metal/water interface.[46,47] At the metal/water interface, H_2 adsorption results in a (solvated) positively charged hydronium ion and a negatively charged metal surface.

Metal particles as an electron reservoir

The preference of heterolytic adsorption as compared to the homolytic adsorption on the bare irreducible oxides is a consequence of the significant band gaps of the oxides (calculated values are presented in the SI). Upon homolytic adsorption, the change from O^{2-} to OH^- creates excess electrons that occupy states in the conduction band of the oxides. A possible way to accommodate the excess electrons is to introduce a metallic phase in the system. The density of states (DOS) for the bare tr-ZrO_2(101) [top] and the Pt/tr-ZrO_2(101) system [bottom] are presented in Fig. 4. The DOS of the bare tr-ZrO_2(101) is related to that of Pt/tr-ZrO_2(101) by aligning the average O(1s) Kohn–Sham eigenvalues in the oxide. On the bare tr-ZrO_2(101) surface, homolytic adsorption results in two excess electrons, residing in the conduction band of the oxide. However, when a Pt NP is supported on the oxide, metallic electronic states are accessible with energies significantly below the conduction band of the oxide. Hence, the Pt NP acts as a potential well and facilitates the homolytic adsorption. Note that the Fermi energy is determined by the NP composition and size. Hence, different metals may facilitate the homolytic adsorption to different extents.

The fundamental origin of the stabilization of hydrogen adsorption in the presence of a metal is the charge transfer from the oxide to the metal. However, the final adsorption energy has several contributions that are visualized in Fig. 5. An O–H bond is created going from 1 → 2 forming an OH^- species and an excess electron. The character of the O–H bond is similar across the different systems as indicated by the small differences in the O–H bond length (see SI). In the absence of a metal NP, the excess charge resides in the conduction band of the oxide surface. As the Fermi energy of the metal is below the edge of the conduction band, energy is gained by charge transfer from the oxide to the metal (2 → 3). One contribution to the adsorption energy is the Coulomb

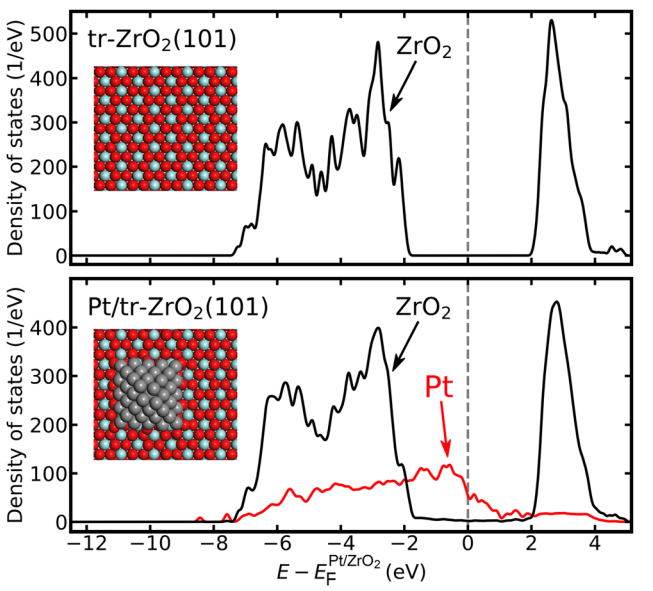

Fig. 4 The density of states for the bare tr-ZrO_2(101) surface [top] and for the Pt_{54}/tr-ZrO_2(101) system [bottom]. The electronic states from tr-ZrO_2 are shown with black, whereas the electronic states of Pt are shown in red. Note that Pt has states above the Fermi energy with energies significantly lower than the conduction band of ZrO_2.

This journal is © The Royal Society of Chemistry 2026

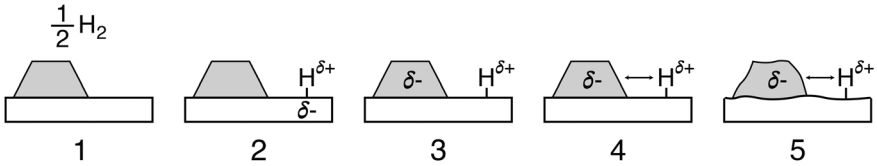

Fig. 5 Deconvolution of the energy contributions associated with homolytic adsorption of hydrogen on the metal/oxide system. 1) is H_2 in the gas phase. 2) is adsorbed H without charge transfer from the oxide to the metal. 3) is adsorbed H with charge transferred to the metal. 4) is the Coulomb interaction between the proton and charged metal nanoparticle. 5) is the structural relaxation owing to the charge transfer.

interaction between the charged metal and H^+ (4). A further contribution to the adsorption energy is the structural relaxation induced by the charge transfer (5). The adhesion between the metal particle and the oxide increases upon hydrogen adsorption, which results in a net stabilization of the adsorption energy.

The character and relative importance of the different contributions to the adsorption energy are system dependent. The strength of the O–H bond depends on the nature of the oxide and location of the excess electrons in (2). Bader analyses show, for example, that the excess electron is delocalized for MgO(100), whereas it is transferred to a neighboring Zr cation for tr-ZrO_2(101). Site resolved Bader analyses are provided in Fig. S20–S22. The energy gain upon charge transfer depends on the relative energy between the oxide conduction band and the Fermi energy of the metal. The DOSes for the pristine metal/oxide systems are reported in Fig. S24 and S25 in the SI. The Coulomb interaction depends on the distance between the metal and the H^+ as well as the localization of charge in the metal. The energy contribution from the structural relaxations are also oxide and metal dependent.

Higher hydrogen coverages on M/ZnO(10$\bar{1}$0)

From Table 1 it is concluded that the homolytic adsorption of H_2 on ZnO(10$\bar{1}$0) is strongly affected by the presence of a metal NP. To investigate the hydrogen adsorption at higher coverages, additional calculation are performed for increasingly more populated ZnO(10$\bar{1}$0) around the metal NPs. In Fig. 6, the average adsorption energy and the total transferred charge as a function of (homolytically) adsorbed H_2 are presented for Cu/ZnO(10$\bar{1}$0) [red], Pd/ZnO(10$\bar{1}$0) [light blue], Pt/ZnO(10$\bar{1}$0) [dark blue], and Au/ZnO(10$\bar{1}$0) [brown]. For comparison, the heterolytic and homolytic adsorption energies on ZnO(10$\bar{1}$0) in the dilute limit are presented with a dashed gray line and a dashed black line, respectively. The average adsorption energy becomes weaker when the number of adsorbed H_2 increases. A weaker adsorption energy at higher coverages is also the case for H_2 adsorption on bare ZnO(10$\bar{1}$0) (see SI), hence, the lateral interactions are substantial. Another reason for the weakened adsorption energy at higher coverages is the monotonic decrease of metal work function at more negatively charged metal NPs (see Fig. S28). As the charge transfer to the NPs stabilizes the homolytic adsorption of H_2 on the oxide, the lower work function results in a weaker adsorption strength. However, even at the highest number of adsorbed H_2 (corresponding to a coverage of roughly 0.5 with respect to the three-fold coordinated oxygen atoms), the adsorption is on average exothermic (Pd, Pt, and Au) or close to thermoneutral (Cu). The slightly weaker adsorption around the Cu NP is in agreement with the lower work function of Cu. The charge transferred to the metal NP upon the adsorption of H_2 on the ZnO(10$\bar{1}$0) surface is monotonically increasing in the entire coverage

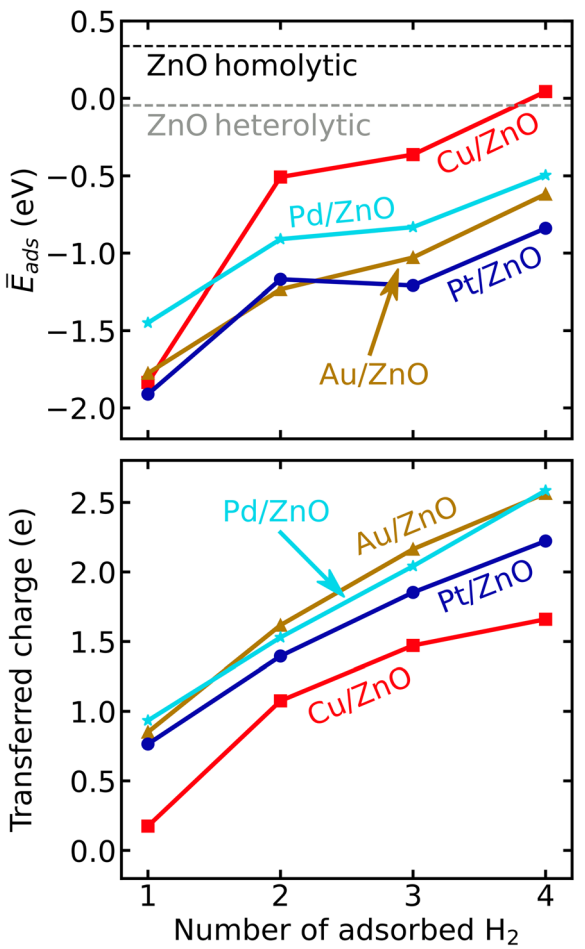

Fig. 6 The average zero-point corrected homolytic adsorption energy of H_2 (top) and the total transferred charge upon the adsorption of H_2 (bottom) on the ZnO(10$\bar{1}$0) surface, with Cu (red), Pd (light blue), Pt (dark blue), and Au (brown) supported on the surface. The gray and black dashed lines represent the heterolytic and homolytic adsorption energies on bare ZnO(10$\bar{1}$0), respectively.

interval for all four metals. The transferred charge per adsorbed H_2 is, however, decreasing at higher coverages, in resemblance with the lower adsorption energies at higher coverages.

Adsorption of H_2 on Pt/MO

The altered adsorption properties of H_2 on ZnO(10$\bar{1}$0) in the presence of a supported metal NP are general, with only a slight metal dependence. To study whether the effects apply also for different irreducible oxide supports, Pt NPs are supported on MgO(100) and tr-ZrO_2(101) surfaces. Fig. 7 shows the optimized adsorption configurations of H_2 (heterolytic and homolytic) on Pt/MgO(100) [top] and Pt/ZrO_2(101) [bottom]. The adsorption energy of H_2 on Pt/MO is presented in black, whereas the corresponding adsorption energy on the bare oxide surface (no Pt NP) is presented in red. The heterolytic adsorption is on MgO(100) and ZrO_2(101) slightly increased in the presence of a supported Pt NP, being 2.11 eV and 0.25 eV, respectively, as compared to 2.03 eV and 0.13 eV on bare MgO(100) and ZrO_2(101), respectively. The heterolytic adsorption is not associated with any significant transfer of charge to the Pt NP. The presence of a Pt NP has significant effects on the homolytic adsorption of H_2. On bare MgO(100), the homolytic adsorption energy is 3.01 eV, whereas the homolytic adsorption energy close to a Pt NP is reduced to 0.85 eV. The adsorption is on Pt/MgO(100) associated with a charge transfer of 1.26 e to the Pt NP. The presence of a supported Pt NP has drastic effects on the homolytic adsorption energy on ZrO_2(101), where the adsorption strength is increased from 2.59 eV (endothermic) to −0.62 eV (exothermic) in the presence of a Pt NP. Also in this case, the adsorption is accompanied by a charge transfer of around 0.9 e to the Pt NP.

The preferred adsorption configuration is reversed for all three oxides in the presence of a supported Pt NP. On bare ZnO(10$\bar{1}$0), MgO(100) and tr-ZrO_2(101) the heterolytic adsorption is favored, whereas the homolytic adsorption on the oxide is favored in the presence of a Pt NP. Note that the homolytic adsorption in the presence of the NP is the only adsorption configuration that would result in any significant H coverages.

Higher hydrogen coverages on Pt/MO

The homolytic adsorption of H_2 on ZnO(10$\bar{1}$0), MgO(100), and tr-ZrO_2(101) is stabilized in the presence of a Pt NP, as a result of a significant charge transfer to the NP. Here, higher hydrogen coverages in the presence of a Pt NP are investigated, Fig. 8. The average adsorption energy decreases with coverage, while the amount of charge transferred to the Pt NP increases monotonically. The magnitude of the transferred charge

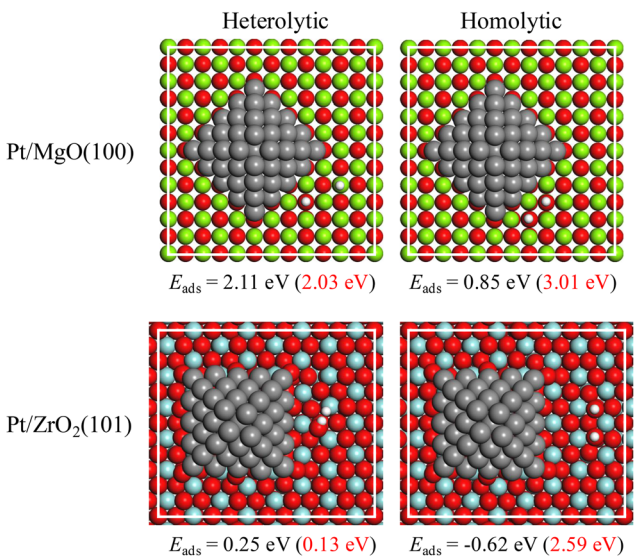

Fig. 7 The optimized adsorption configurations of H_2 for the heterolytic adsorption on Pt/MgO(100) [top left], the homolytic adsorption on Pt/MgO(100) [top right], the heterolytic adsorption on Pt/ZrO_2(101) [bottom left], and the homolytic adsorption on Pt/ZrO_2(101) [bottom right]. The adsorption energies are given in black. As a reference, the corresponding adsorption energies on the bare oxide surfaces are given in red. Atomic color codes: white (H), red (O), green (Mg), light blue (Zr), and gray (Pt).

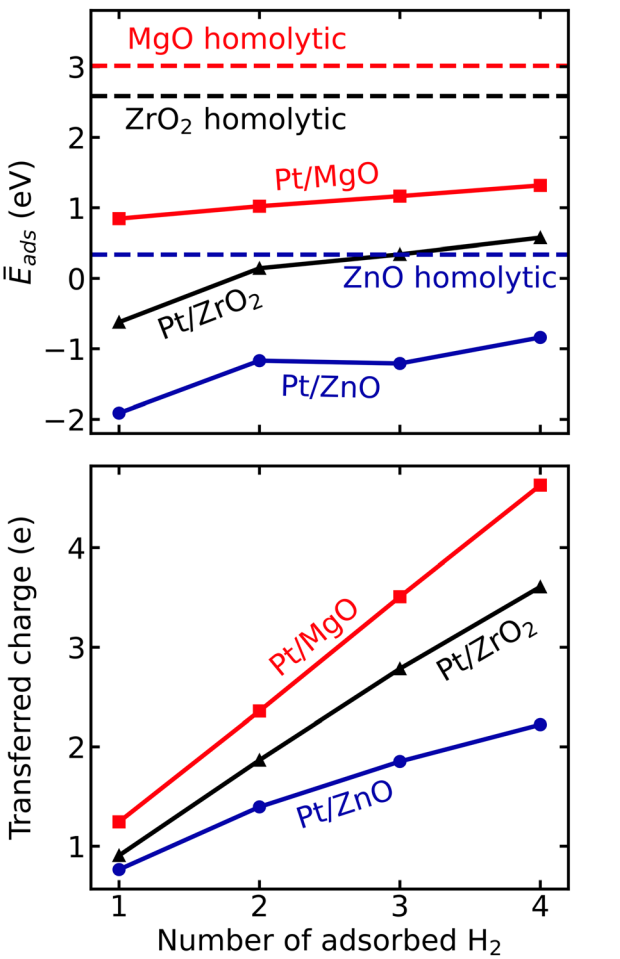

Fig. 8 The average adsorption energy of H_2 (top) and the transferred charge for homolytic adsorption of H_2 (bottom) on the MgO (red), ZrO_2 (black) and ZnO (blue) surfaces, close to a supported Pt NP.

This journal is © The Royal Society of Chemistry 2026

depends on the oxide, being the highest for the more ionic oxide (MgO), and lowest for ZnO. The presence of the Pt NP shift the preferred adsorption configuration from heterolytic, to homolytic for all cases in the low coverage region. The stabilization of homolytically adsorbed H_2 in the presence of a NP ranges between 2.16 eV [MgO(100)] and 2.25 eV [ZnO(10$\bar{1}$0)] to 3.21 eV for tr-ZrO_2(101). In conclusion, the stabilization of the homolytic adsorption of H_2 is general for the investigated metal/oxide systems.

Hydrogen dissociation

The adsorption of hydrogen, from the gas phase to the oxide, may in the metal/oxide systems occur *via* different pathways. Hydrogen could dissociate and adsorb directly on the oxide. Another possibility is that hydrogen dissociates on the metal NP and diffuses (spillover) to the oxide support. To elucidate the most favorable pathway, the two mechanisms are investigated for Cu, Pd and Pt supported on ZnO(10$\bar{1}$0), Fig. 9. The spillover mechanism is investigated also for Cu/ZnO(10$\bar{1}$0) and Pd/ZnO(10$\bar{1}$0). The first step in direct H_2 dissociation on the oxide is physisorption with an energy of −0.19 eV. H_2 dissociates heterolytically on the oxide, with a barrier of 0.63 eV. After dissociating, the hydrogen atom bound to the Zn-cation diffuses to an O-anion, with a barrier 1.09 eV, resulting in a homolytic adsorption configuration. The homolytic adsorption configuration is exothermic with respect to gas phase H_2 (the weaker adsorption strength as compared to the results in Table 1 is a result of non-equivalent adsorption sites). The energy barriers for the mechanism is not significantly affected by the presence of the Pt NP. On bare ZnO(10$\bar{1}$0), the heterolytic dissociation is associated with a barrier of 0.57 eV and the diffusion of H to the homolytic configuration has a barrier of 1.24 eV. However, the final homolytic adsorption configuration is less stable (Table S9 and Fig. S15–S18).

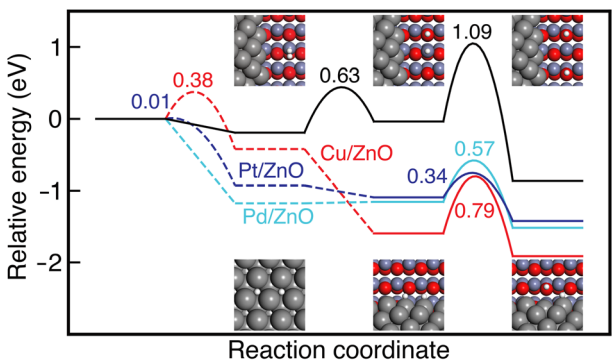

Fig. 9 Two possible pathways in the dissociation of H_2. Heterolytic hydrogen dissociation on the oxide phase of Pt/ZnO, followed by the diffusion of H, resulting in a final homolytic adsorption configuration (black). A spillover mechanism where hydrogen dissociates on the metal NP and diffuses to the oxide support for Pt (dark blue), Cu (red), and Pd (light blue) supported on ZnO. Atomic structures for the case of Pt/ZnO are visualized. Atomic color codes: white (H), red (O), blue (Zn), and gray (Pt).

The alternative paths in Fig. 9 show the spillover mechanism for Cu, Pd, and Pt supported on ZnO(10$\bar{1}$0). The dissociation of H_2 is calculated to have a small barrier (0.01 eV) on Pt(111). The small barrier is in agreement with experimental results.[48] The adsorption energy of 2H adsorbed in fcc hollow sites is −0.93 eV. The adsorption energy of 2H on the perimeter of the Pt NP is −1.09 eV. The diffusion of H from the Pt NP perimeter to ZnO(10$\bar{1}$0) is exothermic, and associated with a barrier of 0.34 eV. The dissociation of H_2 on Cu(111) is exothermic, and associated with a barrier of 0.38 eV. The diffusion of H from the Cu NP perimeter to the ZnO support is exothermic, with a barrier of 0.79 eV. For Pd(111), the dissociation of H_2 is barrierless, and strongly exothermic. The stability of 2H on the perimeter of the Pd NP is similar to the adsorption on Pd(111). The diffusion of H from the Pd NP to the ZnO surface is exothermic, with a barrier of 0.57 eV.

The diffusion of H from the metal NP to ZnO(10$\bar{1}$0) are for all metals exothermic, and associated with lower energy barriers than the direct dissociation of H_2 on ZnO(10$\bar{1}$0). Hence, the spillover mechanism is expected to dominate over the direct dissociation of H_2 on the oxide. The results show that the presence of a metal NP affects both the stability of H adsorbed on the oxide and the kinetics of the dissociation.

Discussion

On the bare metal oxide surfaces; ZnO(10$\bar{1}$0), MgO(100) and tr-ZrO_2(101), hydrogen is preferably adsorbed in (charge conserving) heterolytic configurations, forming $O–H^{\delta+}$ and $M–H^{\delta-}$. The adsorption is in all cases weak, being −0.05 eV, 2.03 eV, and 0.13 eV on ZnO(10$\bar{1}$0), MgO(100), and tr-ZrO_2(101), respectively. The homolytic adsorption, resulting in two O–H and two excess electrons is endothermic on the bare oxides, as the electrons can only reside in the conduction band of the oxide. However, in the presence of a supported metal NP, new electronic states, considerably lower in energy than those in the conduction band of the oxide, are accessible, and the homolytic adsorption is facilitated. In the low coverage region, the homolytic adsorption strength is increased by about 2 eV for ZnO(10$\bar{1}$0) and MgO(100), and more than 3 eV on tr-ZrO_2(101) in the presence of a metal NP. The homolytic adsorption of H_2 on the oxides in the presence of a metal NP is associated with a charge transfer to the NP, that increases with the amount of adsorbed H_2. However, the adsorption strength decreases with the number of adsorbed H_2. The decreased adsorption energy at higher coverages stem from the lateral interactions on the oxide, the lower metal work function as the NP is charged, and less favorable adsorption sites. Energy barrier calculations reveal that the presence of a metal NP influences the kinetics of the hydrogen adsorption, as well as the thermodynamics of the adsorption. The spillover of hydrogen from Cu, Pd, and Pt NPs to the ZnO(10$\bar{1}$0) support are exothermic and associated with barriers of only 0.79 eV, 0.57 eV, and 0.34 eV, respectively. The hydrogen dissociation on the support,

however, is associated with a heterolytic dissociation barrier of 0.63 eV, followed by a diffusion with 1.09 eV barrier to obtain a homolytic adsorption configuration.

The presented results could have important consequences for the understanding of catalytic reactions occurring over metal/oxide composite systems. The stable homolytic adsorption of hydrogen close to the metal NPs results in an oxide region around the NPs that is covered with H. The hydrogen-covered oxide can form hydrogen bonds with intermediates adsorbed on the perimeter of the metal NPs, substantially altering the potential energy landscape, and the catalytic performance. Furthermore, the oxide can, in this case, act as a hydrogen reservoir. The charge transfer upon the homolytic adsorption of H_2 results in negatively charged NPs during reactions conditions, which, *e.g.*, reduces the metal work function. Furthermore, the positively charged H adsorbed close to a negatively charged metal NP results in electric fields. The explored phenomena may influence the stability of intermediates and the energy barriers in catalytic reactions.

Conclusions

We have investigated the hydrogen adsorption on irreducible oxides in the absence and presence of supported metal NPs, to elucidate the underlying reasons for the metal/oxide synergy present in catalytic reactions. On bare ZnO($10\bar{1}0$), MgO(100) and tr-ZrO_2(101), hydrogen is preferably adsorbed heterolytically, and homolytic adsorption (forming 2OH + $2e^-$) is endothermic. However, in the presence of supported metal (Cu, Pd, Pt, and Au) NPs, the excess electrons are transferred to the metal, and the homolytic adsorption is favored over the heterolytic adsorption. Spillover of hydrogen from the metal NPs to the oxide is the dominant mechanism for H_2 adsorption in the case of Cu, Pd, and Pt supported on ZnO($10\bar{1}0$). The increased homolytic adsorption strength is general across the different metal/oxide systems. The increased adsorption strength close to the metal NP results in new interface sites around the NP, where the oxide is populated by hydrogen. The OH-groups could potentially form hydrogen bonds with adsorbates on the NP, or act as a hydrogen reservoir in hydrogenation reactions. The results suggest that nanoparticles supported on irreducible oxides could be negatively charged in hydrogen containing atmospheres, potentially influencing the catalytic activity. The presented results advances the understanding of processes occurring at the metal/oxide interface.

Author contributions

Rasmus Svensson: investigation, formal analysis, writing – original draft, writing – review and editing. Henrik Grönbeck: formal analysis, supervision, writing – review and editing, funding acquisition.

Conflicts of interest

The authors declare no conflicts of interest.

Data availability

The structures are published at Zenodo with the accession code https://doi.org/10.5281/zenodo.20134412.

Supplementary information (SI): atomic models of the considered systems, with calculated values of lattice parameters, surface energies, band gaps, and work functions. Tabulated data of the H_2 adsorption energy, energy barriers, and transferred charge in the different systems. Site-resolved Bader charge difference analyses, densities of states for the investigated systems, and adhesion energy and work functions as a function of H_2 coverage. See DOI: https://doi.org/10.1039/d6cy00643d.

Acknowledgements

Financial support is acknowledged from the Swedish Research Council (2024-05250). The calculations were performed at NSC *via* a NAISS grant (NAISS 2024/3-26). The Competence Centre for Catalysis (KCK) is hosted by Chalmers University of Technology and is financially supported by the Swedish Energy Agency and the member companies Johnson Matthey, Perstorp, Powercell, Preem, Scania CV, Umicore, and Volvo Group.

References

1 T. W. Van Deelen, C. Hernández Mejía and K. P. de Jong, Control of metal-support interactions in heterogeneous catalysts to enhance activity and selectivity, *Nat. Catal.*, 2019, **2**, 955–970.
2 M. Ahmadi, H. Mistry and B. Roldan Cuenya, Tailoring the Catalytic Properties of Metal Nanoparticles via Support Interactions, *J. Phys. Chem. Lett.*, 2016, **7**, 3519–3533.
3 C.-J. Pan, M.-C. Tsai, W.-N. Su, J. Rick, N. G. Akalework, A. K. Agegnehu, S.-Y. Cheng and B.-J. Hwang, Tuning/exploiting Strong Metal-Support Interaction (SMSI) in Heterogeneous Catalysis, *J. Taiwan Inst. Chem. Eng.*, 2017, **74**, 154–186.
4 I. Ro, J. Resasco and P. Christopher, Approaches for Understanding and Controlling Interfacial Effects in Oxide-Supported Metal Catalysts, *ACS Catal.*, 2018, **8**, 7368–7387.
5 P.-A. Carlsson and M. Skoglundh, Low-temperature oxidation of carbon monoxide and methane over alumina and ceria supported platinum catalysts, *Appl. Catal., B*, 2011, **101**, 669–675.
6 K. An, S. Alayoglu, N. Musselwhite, S. Plamthottam, G. Melaet, A. E. Lindeman and G. A. Somorjai, Enhanced CO Oxidation Rates at the Interface of Mesoporous Oxides and Pt Nanoparticles, *J. Am. Chem. Soc.*, 2013, **135**, 16689–16696, PMID: 24090187.
7 D. I. Enache, J. K. Edwards, P. Landon, B. Solsona-Espriu, A. F. Carley, A. A. Herzing, M. Watanabe, C. J. Kiely, D. W. Knight and G. J. Hutchings, Solvent-Free Oxidation of

 This journal is © The Royal Society of Chemistry 2026

Primary Alcohols to Aldehydes Using Au-Pd/TiO_2 Catalysts, *Science*, 2006, **311**, 362–365.
8 J. S. Adams, H. Chen, T. Ricciardulli, S. Vijayaraghavan, A. Sampath and D. W. Flaherty, Distinct Site Motifs Activate O_2 and H_2 on Supported Au Nanoparticles in Liquid Water, *ACS Catal.*, 2024, **14**, 3248–3265.
9 J. A. Boysen, R. Svensson, N. D. Nielsen, M. Lützen, L. Bigom-Eriksen, A. Shavorskiy, T. E. Andersen, J. L. Fischer, J.-C. Grivel, C. D. Damsgaard, A. D. Jensen, H. Grönbeck and J. M. Christensen, Charge Transfer Across the Metal/Oxide Interface Determines the Rate of CO_2 Hydrogenation to Methanol over Cu/ZnO Catalysts, Research Square Preprint, 2026, DOI: 10.21203/rs.3.rs-6939552/v1.
10 J. A. Rodriguez, P. Liu, J. Hrbek, J. Evans and M. Pérez, Water Gas Shift Reaction on Cu and Au Nanoparticles Supported on CeO_2(111) and ZnO(000$\bar{1}$): Intrinsic Activity and Importance of Support Interactions, *Angew. Chem., Int. Ed.*, 2007, **46**, 1329–1332.
11 O. Thinon, F. Diehl, P. Avenier and Y. Schuurman, Screening of bifunctional water-gas shift catalysts, *Catal. Today*, 2008, **137**, 29–35.
12 M. Shekhar, J. Wang, W.-S. Lee, W. D. Williams, S. M. Kim, E. A. Stach, J. T. Miller, W. N. Delgass and F. H. Ribeiro, Size and Support Effects for the Water–Gas Shift Catalysis over Gold Nanoparticles Supported on Model Al_2O_3 and TiO_2, *J. Am. Chem. Soc.*, 2012, **134**, 4700–4708.
13 J. Saavedra, H. A. Doan, C. J. Pursell, L. C. Grabow and B. D. Chandler, The critical role of water at the gold-titania interface in catalytic CO oxidation, *Science*, 2014, **345**, 1599–1602.
14 R. M. Palomino, P. J. Ramírez, Z. Liu, R. Hamlyn, I. Waluyo, M. Mahapatra, I. Orozco, A. Hunt, J. P. Simonovis, S. D. Senanayake and J. A. Rodriguez, Hydrogenation of CO_2 on ZnO/Cu(100) and ZnO/Cu(111) Catalysts: Role of Copper Structure and Metal-Oxide Interface in Methanol Synthesis, *J. Phys. Chem. B*, 2018, **122**, 794–800.
15 T. Daio, A. Staykov, L. Guo, J. Liu, M. Tanaka, S. Matthew Lyth and K. Sasaki, Lattice strain mapping of platinum nanoparticles on carbon and SnO_2 supports, *Sci. Rep.*, 2015, **5**, 13126.
16 T. Nilsson Pingel, M. Jørgensen, A. B. Yankovich, H. Grönbeck and E. Olsson, Influence of atomic site-specific strain on catalytic activity of supported nanoparticles, *Nat. Commun.*, 2018, **9**, 2722.
17 M. Mavrikakis, B. Hammer and J. K. Nørskov, Effect of Strain on the Reactivity of Metal Surfaces, *Phys. Rev. Lett.*, 1998, **81**, 2819–2822.
18 A. Khorshidi, J. Violet, J. Hashemi and A. A. Peterson, How strain can break the scaling relations of catalysis, *Nat. Catal.*, 2018, **1**, 263–268.
19 E. M. Dietze and H. Grönbeck, Structure-Dependent Strain Effects, *ChemPhysChem*, 2020, **21**, 2407–2410.
20 M. García-Melchor and N. López, Homolytic Products from Heterolytic Paths in H_2 Dissociation on Metal Oxides: The Example of CeO_2, *J. Phys. Chem. C*, 2014, **118**, 10921–10926.
21 H.-Y. T. Chen, L. Giordano and G. Pacchioni, From Heterolytic to Homolytic H_2 Dissociation on Nanostructured MgO(001) Films As a Function of the Metal Support, *J. Phys. Chem. C*, 2013, **117**, 10623–10629.
22 R. Eischens, W. Pliskin and M. Low, The infrared spectrum of hydrogen chemisorbed on zinc oxide, *J. Catal.*, 1962, **1**, 180–191.
23 F. Boccuzzi, E. Borello, A. Zecchina, A. Bossi and M. Camia, Infrared study of ZnO surface properties: I. Hydrogen and deuterium chemisorption at room temperature, *J. Catal.*, 1978, **51**, 150–159.
24 T. Ito, M. Kuramoto, M. Yoshioka and T. Tokuda, Active sites for hydrogen adsorption on magnesium oxide, *J. Phys. Chem.*, 1983, **87**, 4411–4416.
25 J. Kondo, Y. Sakata, K. Domen, K.-i. Maruya and T. Onishi, Infrared study of hydrogen adsorbed on ZrO_2, *J. Chem. Soc., Faraday Trans.*, 1990, **86**, 397–401.
26 D. Fernández-Torre, J. Carrasco, M. V. Ganduglia-Pirovano and R. Pérez, Hydrogen activation, diffusion, and clustering on CeO_2(111): A DFT+U study, *J. Chem. Phys.*, 2014, **141**, 014703.
27 K. Honkala, A. Hellman and H. Grönbeck, Water Dissociation on MgO/Ag(100): Support Induced Stabilization or Electron Pairing?, *J. Phys. Chem. C*, 2010, **114**, 7070–7075.
28 H. V. Thang and G. Pacchioni, H_2 Adsorption on Wurtzite ZnO and on ZnO/M(111) (M=Cu, Ag and Au) Bilayer Films, *ChemNanoMat*, 2019, **5**, 932–939.
29 G. Kresse and J. Hafner, Ab initio molecular dynamics for liquid metals, *Phys. Rev. B: Condens. Matter Mater. Phys.*, 1993, **47**, 558–561.
30 G. Kresse and J. Hafner, Ab initio molecular dynamics for open-shell transition metals, *Phys. Rev. B: Condens. Matter Mater. Phys.*, 1993, **48**, 13115–13118.
31 G. Kresse and J. Hafner, Ab initio molecular-dynamics simulation of the liquid-metal–amorphous-semiconductor transition in germanium, *Phys. Rev. B: Condens. Matter Mater. Phys.*, 1994, **49**, 14251–14269.
32 G. Kresse and J. Furthmüller, Efficient iterative schemes for ab initio total-energy calculations using a plane-wave basis set, *Phys. Rev. B: Condens. Matter Mater. Phys.*, 1996, **54**, 11169–11186.
33 P. E. Blöchl, Projector augmented-wave method, *Phys. Rev. B: Condens. Matter Mater. Phys.*, 1994, **50**, 17953–17979.
34 G. Kresse and D. Joubert, From ultrasoft pseudopotentials to the projector augmented-wave method, *Phys. Rev. B: Condens. Matter Mater. Phys.*, 1999, **59**, 1758–1775.
35 J. P. Perdew, K. Burke and M. Ernzerhof, Generalized gradient approximation made simple, *Phys. Rev. Lett.*, 1996, **77**, 3865–3868.
36 S. L. Dudarev, G. A. Botton, S. Y. Savrasov, C. J. Humphreys and A. P. Sutton, Electron-energy-loss spectra and the structural stability of nickel oxide: An LSDA+U study, *Phys. Rev. B: Condens. Matter Mater. Phys.*, 1998, **57**, 1505–1509.
37 P. Erhart, K. Albe and A. Klein, First-principles study of intrinsic point defects in ZnO: Role of band structure, volume relaxation, and finite-size effects, *Phys. Rev. B: Condens. Matter Mater. Phys.*, 2006, **73**, 205203.
38 H.-Y. T. Chen, S. Tosoni and G. Pacchioni, Adsorption of Ruthenium Atoms and Clusters on Anatase TiO_2 and

Tetragonal ZrO_2(101) Surfaces: A Comparative DFT Study, *J. Phys. Chem. C*, 2015, **119**, 10856–10868.
39 G. Henkelman, A. Arnaldsson and H. Jónsson, A fast and robust algorithm for Bader decomposition of charge density, *Comput. Mater. Sci.*, 2006, **36**, 354–360.
40 G. Henkelman and H. Jónsson, Improved tangent estimate in the nudged elastic band method for finding minimum energy paths and saddle points, *J. Chem. Phys.*, 2000, **113**, 9978–9985.
41 G. Henkelman, B. P. Uberuaga and H. Jónsson, A climbing image nudged elastic band method for finding saddle points and minimum energy paths, *J. Chem. Phys.*, 2000, **113**, 9901–9904.
42 G. Pacchioni, L. Giordano and M. Baistrocchi, Charging of Metal Atoms on Ultrathin MgO/Mo(100) Films, *Phys. Rev. Lett.*, 2005, **94**, 226104.
43 H. Grönbeck, Mechanism for NO_2 Charging on Metal Supported MgO, *J. Phys. Chem. B*, 2006, **110**, 11977–11981.
44 M. Sterrer, T. Risse, U. Martinez Pozzoni, L. Giordano, M. Heyde, H.-P. Rust, G. Pacchioni and H.-J. Freund, Control of the Charge State of Metal Atoms on Thin MgO Films, *Phys. Rev. Lett.*, 2007, **98**, 096107.
45 Y.-N. Sun, L. Giordano, J. Goniakowski, M. Lewandowski, Z.-H. Qin, C. Noguera, S. Shaikhutdinov, G. Pacchioni and H.-J. Freund, The Interplay between Structure and CO Oxidation Catalysis on Metal-Supported Ultrathin Oxide Films, *Angew. Chem., Int. Ed.*, 2010, **49**, 4418–4421.
46 R. Svensson and H. Grönbeck, Site Communication in Direct Formation of H2O2 over Single-Atom Pd@Au Nanoparticles, *J. Am. Chem. Soc.*, 2023, **145**, 11579–11588.
47 R. Svensson and H. Grönbeck, Spontaneous Charge Separation at the Metal-Water Interface, *ChemPhysChem*, 2024, **25**, e202400099.
48 K. Christmann, G. Ertl and T. Pignet, Adsorption of hydrogen on a Pt(111) surface, *Surf. Sci.*, 1976, **54**, 365–392.

 This journal is © The Royal Society of Chemistry 2026